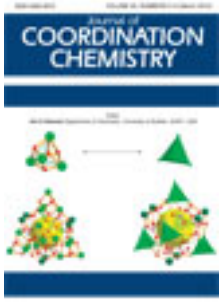


Journal of Coordination Chemistry
Publication details, including instructions for authors and subscription information:
http://www.tandfonline.com/loi/gcoo20

# Molecular structures of antitumor active Pd(II) and Pt(II) complexes of N,N-donor benzimidazole methyl ester

N.T. Abdel-Ghani [a] & A.M. Mansour [a]
[a] Chemistry Department, Faculty of Science , Cairo University , Gamaa Street, Giza 12613 , Egypt
Published online: 15 Feb 2012.

To cite this article: N.T. Abdel-Ghani & A.M. Mansour (2012) Molecular structures of antitumor active Pd(II) and Pt(II) complexes of N,N-donor benzimidazole methyl ester, Journal of Coordination Chemistry, 65:5, 763-779, DOI: 10.1080/00958972.2012.661048

To link to this article: http://dx.doi.org/10.1080/00958972.2012.661048

*Journal of Coordination Chemistry*
Vol. 65, No. 5, 10 March 2012, 763–779



# Molecular structures of antitumor active Pd(II) and Pt(II) complexes of *N*,*N*-donor benzimidazole methyl ester

N.T. ABDEL-GHANI* and A.M. MANSOUR

Chemistry Department, Faculty of Science, Cairo University, Gamaa Street, Giza 12613, Egypt

(*Received 26 August 2011; in final form 23 December 2011*)

$[MLCl_2]\cdot zH_2O\cdot C_2H_5OH$ (L = 2-[(1H-benzimidazol-2-ylmethyl)-amino]-benzoic acid methyl ester; M = Pd, z = 2; M = Pt, z = 0) complexes were synthesized as potential antitumor compounds and their structures were elucidated by elemental analysis and spectroscopic data. Theoretical molecular structures were investigated by the DFT/B3LYP method using the LANL2DZ basis set. The calculated molecular parameters, bond distances, and angles, revealed a square-planar geometry around the metal through pyridine-type nitrogen ($N_{py}$) of benzimidazole and the secondary amino group ($NH_{sec}$). The lone pair interaction LP(2)O48 of ethanol with anti-bonding $\sigma^*$(C(16)–H(29)) is an evidence for charge transfer from ethanol to platinum. The electronic movement and assignment of electronic spectra were carried out by TD-DFT calculations. The ligand in comparison to its metal complexes was screened for antibacterial activity and cytotoxicity.

*Keywords*: Benzimidazole; Hydrogen bonding; TD-DFT; NBO; Cytotoxicity



## 1. Introduction

Despite the extensive clinical use of *cis*-platin against several types of cancers, its severe side effects make the development of new drugs crucial [1]. The most intensively studied compounds in this respect are *cis*-$[PtCl_2L_2]$ complexes, where $L_2$ is a ligand coordinated to the metal through two nitrogen atoms. Recently, interest has been directed towards developing *cis*-platin analogues with heterocyclic amine ligands [2], e.g., benzimidazole. The benzimidazole scaffold has potent biological activities as antitumor, anti-HIV, and antimicrobial agents [3]. At the same time, owing to coordination ability of azoles, chelating ligands incorporating benzimidazole groups were extensively studied in the context of modeling biological systems [4]. Palladium complexes have also received considerable interest because of the structural analogy between Pt(II) and Pd(II) complexes. The design of Pd(II) compounds with an anticancer activity represents an exciting task, since Pd(II) compounds exchange ligands 105 times faster than the analogous Pt(II) compounds [5]. Recently, structural studies, antimicrobial, *in vitro* cytotoxicity, and structure–activity relationship of related 2-arylaminomethylbenzimidazole derivatives and their metal complexes were

*Corresponding author. Email: noureta2002@yahoo.com


ISSN 0095-8972 print/ISSN 1029-0389 online 
http://dx.doi.org/10.1080/00958972.2012.661048

reported [2]. Pd(II) and Pt(II) complexes have square-planar geometry through NNH donor sites. However, the palladium complexes were inactive against all the tested Gram-positive and Gram-negative bacteria, whatever the nature of the substituent in the *para*-position of the aniline ring [2].

As continuation of our recent studies on the synthesis, structural investigations, and antitumor activities of some benzimidazole metal complexes, the main aspects of the present study are: (i) to discuss the coordination mode of a new benzimidazole derivative with $-COOCH_3$ at the *ortho*-position on aniline (figure 1), which could make a potential tridentate ligand as compared to bidentate ligands of *para*-functionalized derivatives reported in previous studies [2]; (ii) to examine how introduction of an ester group in the *ortho*-position affects the biological activity of the ligand and its complexes; (iii) theoretical studies of the complexes with one ethanol molecule in terms of intermolecular interactions.



## 2. Experimental

### 2.1. *Synthesis of the ligand (L) and its complexes*

All chemicals used in this study were of reagent grade (Sigma). The benzimidazole L (figure 1) was prepared as previously published [6]. The solid Pd(II) and Pt(II) complexes were prepared by adding a hot ethanolic solution (60°C) of the ligand L (1 mmol) to a hot aqueous solution (60°C) of the metal ions (1 mmol; $K_2PdCl_4$ or $K_2PtCl_4$). The resulting mixtures were stirred under reflux for 1–2 h, whereupon the complexes were precipitated.

Data for **L** ($C_{16}H_{15}N_3O_2$) [6]. Color: Yellow. MS: $M^+$ 281 (Calcd 281.31), 248, 220, 131, and 118. Anal Calcd for $C_{16}H_{15}N_3O_2$ (%): C, 68.31; H, 5.37; N, 14.94. Found (%): C, 67.94; H, 5.00; N, 14.80. FT-IR: 3345 ($\nu(NH)_{sec}$), 2987 ($\nu(CH_3)_{ass}$), 2950 ($\nu(CH_3)_{ss}$), 2831 ($\nu(CH_2)$), 1674 ($\nu(C{=}O)$), 1581 ($\nu(C{=}C)$), 1512 ($\nu(C{=}C)$), 1447 ($\beta(NH)_{sec}$), 1323 ($\nu(C{-}N)_{sec}$), and 1235 $cm^{-1}$ ($\nu(C{-}O)$). $^1$H-NMR (DMSO): $\delta$ 12.35 (1H, s, benzimidazolic NH); $\delta$ 6.64 (1H, t, $H^{34}$), $\delta$ 6.76 (1H, d, $H^{35}$), $\delta$ 7.35 (1H, t, $H^{33}$), $\delta$ 7.83 (1H, d, $H^{32}$); $\delta$ 7.14, 7.15, 7.40, 7.58 (4H, m, benzimidazole ring (Bz) protons ($H^{7-10}$)), $\delta$ 8.30 (1H, t, secondary amino proton (sec)), $\delta$ 4.68 (2H, d, $CH_2$ protons), and $\delta$ 3.80 (3H, s, $CH_3$ protons). UV-Vis (DMF): 263, 275, 281, 340 nm.

Data for **Pd–L** ($C_{18}H_{25}Cl_2N_3O_5Pd$). Color: Yellow. MS: $m/z$ 310, [Pd(benzimidazole)$CH_2Cl_2$]; 295, [Pd(benzimidazole)$Cl_2$]. Anal. Calcd for $C_{18}H_{25}Cl_2N_3O_5Pd$ (%): C, 39.98; H, 4.66; N, 7.77; Pd, 19.68. Found (%): C, 41.09; H, 5.19; N, 7.14; Pd, 18.03. FT-IR: 3352 ($\nu(NH)_{sec}$), 1688 ($\nu(C{=}O)$), 1605 ($\nu(C{=}C)$), 1503 ($\nu(C{=}C)$), 1447 ($\beta(NH)_{sec}$), and 1273 $cm^{-1}$ ($\nu(C{-}O)$). $^1$H-NMR (DMSO): $\delta$ 13.27 (1H, s, $NH_{Bz}$); $\delta$ 6.63–8.08 (8H, m, aromatic protons), $\delta$ 8.50 (1H, t, $NH_{sec}$), $\delta$ 5.23 (2H, d, $CH_2$ protons), $\delta$ 4.36 (2H, m, $CH_2$ of ethanol), $\delta$ 3.86 (3H, s, $CH_3$ protons), $\delta$ 3.33 (1H, t, OH of ethanol), $\delta$ 3.21 (4H, s, $H_2O$), and $\delta$ 1.34 (3H, t, $CH_3$ of ethanol). UV-Vis. (DMF): 273, 279, 347, 434, and 465 nm. Molar Cond. ($10^{-3}$, DMF): 13.96 $\Omega^{-1}\,cm^2\,mol^{-1}$.

Data for **Pt–L** ($C_{18}H_{21}Cl_2N_3O_3Pt$). Color: Brown. MS: $M^+ = 546$, M–$C_2H_5OH$ (Calcd 592); 497, M–Cl–$CH_3$–$C_2H_5OH$; 450, M–Cl–$CH_3$–$CO_2$–$C_2H_5OH$. Anal. Calcd for $C_{18}H_{21}Cl_2N_3O_3Pt$ (%): C, 36.44; H, 3.57; N, 7.08; Pt, 32.88. Found (%): C, 36.60;

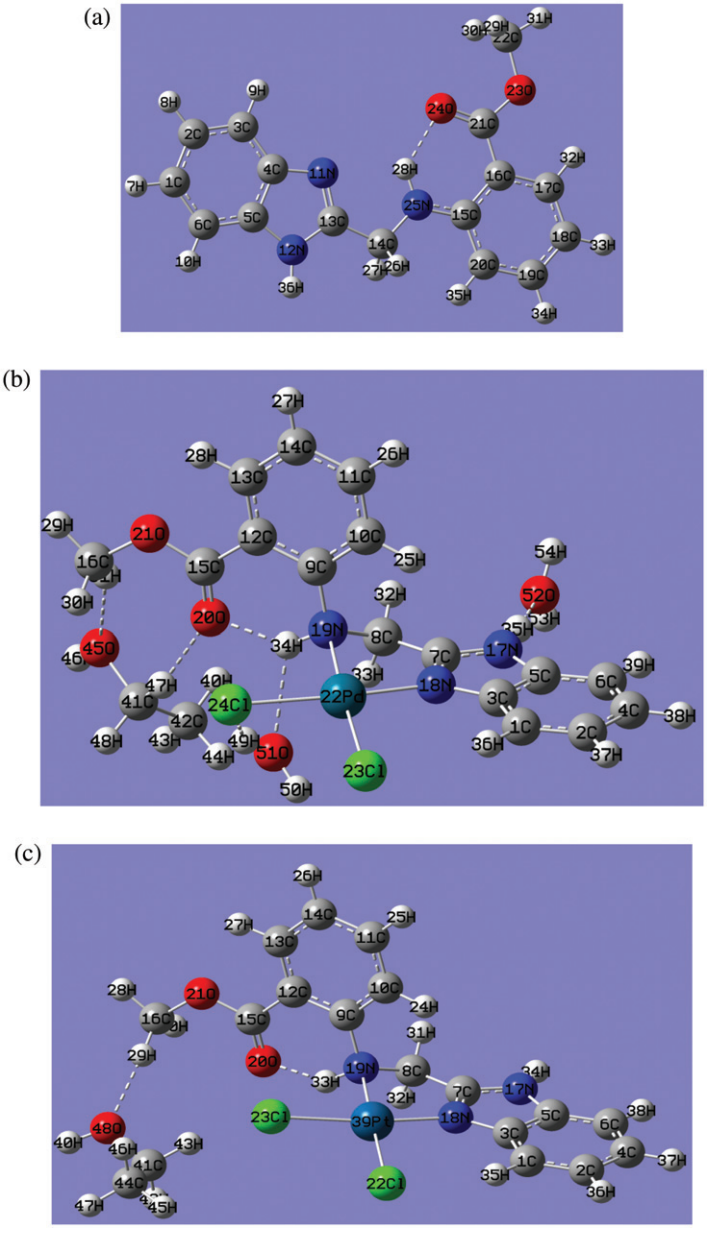


Figure 1. The optimized structures of (a) benzimidazole L, (b) *cis*-$[PdLCl_2]\cdot 2H_2O\cdot C_2H_5OH$, and (c) *cis*-$[PtLCl_2]\cdot C_2H_5OH$.

H, 3.57; N, 7.11; Pt, 32.79. FT-IR: 3375 ($\nu(NH)_{sec}$), 1674 ($\nu(C{=}O)$), 1581 ($\nu(C{=}C)$), 1509 ($\nu(C{=}C)$), 1447 ($\beta(NH)_{sec}$), and 1267 $cm^{-1}$ ($\nu(C{-}O)$). $^1$H-NMR (DMSO): $\delta$ 13.36 (1H, s, $NH_{Bz}$); $\delta$ 6.61–8.08 (8H, m, aromatic protons), $\delta$ 8.41 (1H, t, $NH_{sec}$), $\delta$ 5.24 (2H, d, $CH_2$ protons), $\delta$ 4.32 (2H, m, $CH_2$ of ethanol), $\delta$ 3.88 (3H, s, $CH_3$ protons), $\delta$ 3.18 (1H, t, OH of ethanol), and $\delta$ 1.36 (3H, t, $CH_3$ of ethanol). UV-Vis. (DMF): 274, 280, 345, and 416 nm. Molar Cond. ($10^{-3}$, DMF): 12.75 $\Omega^{-1}\,cm^2\,mol^{-1}$.

### 2.2. *Instruments*

Infrared (IR) spectra were recorded as KBr pellets using FTIR-460 plus, JASCO, from 4000 to 200 $cm^{-1}$. $^1$H-NMR spectra were run at 300 MHz in DMSO-$d_6$ using a Varian-Oxford Mercury VX-300 NMR. Mass spectra were recorded with a SHIMADZU QP-2010 plus mass spectrometer at 70 eV. The X-ray powder diffraction patterns were recorded over $2\theta = 5$–$60^\circ$ using a Philips X-ray diffractometer model PW 1840. Radiation was provided by copper anode (K$\alpha$, $\lambda = 1.54056$ Å) operated at 40 kV and 25 mA. Thermal analyses (TG/DTA) were carried out in a dynamic nitrogen atmosphere (20 mL $min^{-1}$) with a heating rate of 10°C $min^{-1}$ in platinum crucibles using a DTG-60 H Simultaneous DTA-TG Apparatus – Shimadzu. Elemental microanalyses (C, H, and N) were performed at the Micro-analytical Center, Cairo University. The analyses were repeated twice to check the accuracy of the analyzed data. The metal content was determined gravimetrically [7]. Digital Jenway 4330 Conductivity-pH meter with (1.02) cell constant was used for pH and molar conductance measurements. The UV-Vis. measurements were carried out using an automated spectrophotometer UV-Vis. Shimadzu Lambda 4B using 1 cm matched quartz cells.

### 2.3. *Computational details*

The gas phase geometries of $[PdLCl_2] \cdot 2H_2O \cdot C_2H_5OH$ and $[PtLCl_2] \cdot C_2H_5OH$ were optimized by the DFT/B3LYP method [8]. The effective core potential (ECP) of Hay and Wadt and the LanL2DZ basis were used [9]. Calculations were carried out using *GAUSSIAN 03* [10]. The optimized geometries were verified by performing a frequency calculation. Vibrational modes were analyzed using *GAUSSVIEW* software [11]. The electronic spectra were obtained using time-dependent density functional theory (TD-DFT) [12]. Net atomic charges were obtained using the natural bond orbital (NBO) analysis of Weinhold and Carpenter [13]. Frontier molecular orbitals (FMO) were performed at the same level of theory.

### 2.4. *Biological activity*

**2.4.1. Antimicrobial activity.** The antimicrobial activities of the test samples were determined by a modified Kirby–Bauer disc diffusion method [14] under standard conditions using the Mueller–Hinton agar medium (tested for composition and pH), as described by NCCLS [15]. The antimicrobial activities were carried out using the culture of *Bacillus subtilis*, *Staphylococcus aureus*, and *Streptococcus faecalis* as Gram-positive bacteria and *Escherichia coli*, *Pseudomonas aeruginosa*, and *Neisseria gonorrhea* as Gram-negative bacteria. Solution of 100 mg $mL^{-1}$ of each compound (studied compounds and standard drug *Tetracycline*) in DMSO was prepared for testing against bacteria. Centrifuged pellets of bacteria from a 24 h-old culture containing $10^4$–$10^6$ colony forming unit (CFU) per mL were spread on the surface of Muller Hinton agar plates. Then the wells were seeded with 10 mL of the prepared inocula to have $10^6$ CFU $mL^{-1}$. Petri plates were prepared by pouring 100 mL of seeded nutrient agar. DMSO (0.1 mL) alone was used as a control under the same conditions for each microorganism, subtracting the diameter of inhibition zone resulting

with DMSO, from that obtained in each case. The antimicrobial activities were calculated as a mean of three replicates.

**2.4.2. Cell culture and cytotoxicity determination.** Three human cancer cell lines were used for *in vitro* screening experiments; *breast cancer* (MCF7), *colon carcinoma* (HCT), and *human heptaocellular carcinoma* ($HepG_2$). They were obtained frozen in liquid nitrogen (−180 °C) from the American Type Culture Collection. The tumor cell lines were maintained in the National Cancer Institute, Cairo, Egypt, by serial sub-culturing. Potential cytotoxicities of the compounds were tested using the Skehan *et al.* method [16]. Cells were plated in 96-multiwell plates ($5 \times 10^3$–$4 \times 10^4$ cells/well) for 24 h before treatment with the compounds to allow the attachment of cell to the wall of the plate. RPMI-1640 medium (5% fetal bovine serum and 2 mmol $L^{-1}$ L-glutamine) was used for culturing and maintenance of the human tumor cell lines [17]. Different concentrations (50 and 100 μmol $L^{-1}$) of the compounds under study were added to the cell monolayer triplicate wells prepared for each individual dose. The monolayer cells were incubated with the compounds for 48 h at 37°C and in 5% $CO_2$ atmosphere. After 48 h, cells were fixed, washed, and stained with the protein-binding dye sulforhodamine B (SRB) [16]. Excess stain was washed with acetic acid and attached stain was recovered with tris-EDTA buffer. The optical density (OD) of each well was measured spectrophotometrically at 564 nm with an ELIZA microplate reader and the mean background absorbance was automatically subtracted and mean values of each drug concentration was calculated. The relation between surviving fraction and drug concentration is plotted to get the survival curve. The results were compared with a similar run of *cis*-platin as an antitumor compound.



## 3. Results and discussion

### 3.1. *Geometry optimization*

The fully optimized geometries of L, *cis*-$[PdLCl_2] \cdot 2H_2O \cdot C_2H_5OH$, and *cis*-$[PtLCl_2] \cdot C_2H_5OH$ and numbering of atoms are shown in figure 1. The coordination sphere around the metal center in these complexes is made up of $N_{py}$, $NH_{sec}$, and two chlorides completing the square-planar geometry. The coordination centers are coplanar, whereas the phenyl ring is bent out of the plane by 94.056° (Pd–L) and 104.42° (Pt–L) complexes. This behavior prevents participation of the carbonyl in coordination as found experimentally; this will be confirmed later. As shown in table 1, the M–$NH_{sec}$ bond length is about 4.62% longer than M–$N_{py}$ bond distance [18]. In addition, the bond lengths Pd–$NH_{sec}$ (2.161 Å) and Pd–$N_{py}$ (2.066 Å) in the $[PdLCl_2] \cdot 2H_2O \cdot C_2H_5OH$ complex are longer than the Pt–$NH_3$ bond in *cis*-platin by 0.151 and 0.056 Å, respectively, and these bonds are shorter than those previously published (Pd–$L^1$, $L^1$ = (1H-benzimidazol-2-ylmethyl)-(4-nitro-phenyl)-amine), by 2.070 and 2.186 Å, respectively [2]. This may be interpreted in terms of the nature and position of the substituent on the aniline, where the presence of nitro [2] in the *para* position decreases the coordinating ability of the secondary amino group toward the metal ion and thus lengthens these bond distances. Pd–Cl(23) and Pd–Cl(24) bond distances in the Pd–L complex are longer than those of the platinum complex by 0.046

Table 1. Selected bond lengths (Å), angles (°), and charges for *cis*-[$PdLCl_2$]·$C_2H_5OH$·$2H_2O$ and *cis*-[$PtLCl_2$]·$C_2H_5OH$.

| *cis*-[$PdLCl_2$]·$C_2H_5OH$·$2H_2O$ | | | | | *cis*-[$PtLCl_2$]·$C_2H_5OH$ | | | | |
|---|---|---|---|---|---|---|---|---|---|
| Bond lengths (Å) | | Bond angles (°) | | Charge (e) | Bond lengths (Å) | | Bond angles (°) | | Charge (e) |
| C1C2 | 1.403 | C1C2C4 | 121.745 | C1 = −0.194 | C1C2 | 1.403 | C1C2C4 | 121.817 | C1 = −0.186 |
| C1C3 | 1.407 | C2C4C6 | 121.523 | C2 = −0.219 | C1C3 | 1.406 | C2C4C6 | 121.515 | C2 = −0.214 |
| C3C5 | 1.427 | C4C6C5 | 116.738 | C3 = 0.150 | C3C5 | 1.425 | C4C6C5 | 116.537 | C3 = 0.153 |
| C5C6 | 1.405 | C6C5C3 | 121.937 | C4 = −0.208 | C5C6 | 1.404 | C6C5C3 | 122.244 | C4 = −0.199 |
| C4C6 | 1.404 | C1C3C5 | 120.947 | C5 = 0.149 | C4C6 | 1.404 | C1C3C5 | 120.839 | C5 = 0.154 |
| C2C4 | 1.422 | C2C1C3 | 117.111 | C6 = −0.249 | C2C4 | 1.421 | C2C1C3 | 117.048 | C6 = −0.251 |
| C3N18 | 1.410 | C3N18C7 | 107.106 | C7 = 0.484 | C3N18 | 1.414 | C3N18C7 | 107.457 | C7 = 0.482 |
| C5N17 | 1.406 | C5N17C7 | 107.331 | C8 = −0.248 | C5N17 | 1.409 | C5N17C7 | 107.786 | C8 = −0.246 |
| C7N18 | 1.343 | N18C7N17 | 111.770 | C9 = 0.212 | C7N18 | 1.339 | N17C7N18 | 111.170 | C9 = 0.208 |
| C7N17 | 1.370 | C7C8N19 | 109.413 | C10 = −0.234 | C7N17 | 1.376 | C7C8N19 | 109.029 | C10 = −0.230 |
| C7C8 | 1.498 | N18PdN19 | 81.131 | C11 = −0.173 | C7C8 | 1.498 | N18PtN19 | 81.597 | C11 = −0.171 |
| C8N19 | 1.509 | Cl23PdCl24 | 92.969 | C12 = −0.168 | C8N19 | 1.518 | Cl22PtCl23 | 91.634 | C12 = −0.167 |
| C9N19 | 1.459 | C8N19C9 | 116.291 | C13 = −0.154 | C9N19 | 1.472 | C8N19C9 | 114.292 | C13 = −0.153 |
| C9C10 | 1.409 | N19C9C12 | 121.047 | C14 = −0.215 | C9C10 | 1.405 | N19C9C12 | 120.372 | C14 = −0.210 |
| C10C11 | 1.403 | N19C9C10 | 119.550 | C15 = 0.845 | C10C11 | 1.403 | N19C9C10 | 119.485 | C15 = 0.844 |
| C11C14 | 1.409 | C9C12C13 | 119.212 | C16 = −0.267 | C11C14 | 1.409 | C9C12C13 | 118.925 | C16 = −0.266 |
| C13C14 | 1.401 | C12C13C14 | 121.013 | N17 = −0.602 | C13C14 | 1.401 | C12C13C14 | 120.826 | N17 = −0.599 |
| C12C13 | 1.414 | C11C14C13 | 119.459 | N18 = −0.536 | C12C13 | 1.414 | C11C14C13 | 119.697 | N18 = −0.520 |
| C9C12 | 1.424 | C10C11C14 | 120.312 | N19 = −0.675 | C9C12 | 1.420 | C10C11C14 | 120.214 | N19 = −0.676 |
| C12C15 | 1.490 | C9C10C11 | 120.604 | O20 = −0.657 | C12C15 | 1.492 | C9C10C11 | 120.190 | O20 = −0.663 |
| C15O20 | 1.255 | C10C9C12 | 119.388 | O21 = −0.568 | C15O20 | 1.260 | C10C9C12 | 120.131 | O21 = −0.561 |
| C15O21 | 1.363 | C9C12C15 | 121.327 | Pd = 0.342 | C15O21 | 1.357 | C9C12C15 | 121.300 | Pt = 0.311 |
| C16O21 | | O20C15O21 | 122.181 | Cl23 = −0.404 | C16O21 | 1.488 | O20C15O21 | 122.421 | Cl22 = −0.398 |
| N18Pd | 2.066 | C15O21C16 | 117.312 | Cl24 = −0.444 | N18Pt | 2.045 | C15O21C16 | 117.815 | Cl23 = −0.423 |
| N19Pd | 2.161 | | | H34 = 0.232 | N19Pt | 2.130 | | | H33 = 0.483 |
| Cl23Pd | 2.376 | | | H35 = 0.227 | Cl22Pt | 2.403 | | | H34 = 0.443 |
| Cl24Pd | 2.403 | | | O45 = −0.815 | Cl23Pt | 2.408 | | | |
| | | | | H49 = 0.503 | | | | | |
| O20H34 | 1.825 | | | | O20H33 | 1.782 | | | |
| O52H35 | 1.725 | | | | O48H29 | 2.133 | | | |
| O45H31 | 2.314 | | | | O20H43 | 3.053 | | | |
| O20H47 | 2.281 | | | | | | | | |
| Cl24H49 | 2.393 | | | | | | | | |
| E (a.u.) | | | | −1397.968 | | | | −1237.518 | |
| Zero-point E (kcal mol−$^{1}$) | | | | 266.015 | | | | 236.026 | |
| Rotational constants (GHz) | | | | 0.163, 0.077, 0.075 | | | | 0.216, 0.090, 0.075 | |
| Entropy (cal mol−$^{1}$ K−$^{1}$) | | | | | | | | | |
| Translational | | | 44.739 | | | 45.019 | | | |
| Rotational | | | 37.085 | | | 36.641 | | | |
| Vibrational | | | 151.650 | | | 119.357 | | | |
| Total Dipole moment (D) | | | 17.190 | | | 13.165 | | | |

and 0.073 Å, respectively, owing to the *trans*-influence. The C(8)N(19) and C(9)N(19) bond lengths in the Pd–L complex were increased by 0.056 and 0.082 Å, respectively, compared to those of the free ligand due to participation of the $NH_{sec}$ group in the coordination sphere of the complex. The Pd–$N_{py}$ (2.066 Å) and Pd–$NH_{sec}$ (2.161 Å) distances are in agreement with those observed in benzimidazole complexes [19]. Moreover, the Pt–$N_{py}$ and Pt–$NH_{sec}$ bond distances are shorter than that of the Pd–L complex by 0.021 and 0.031 Å, respectively, due to the size of the metal ion. The optimized N(18)–Pd–N(19) (81.131°) angle is smaller than that of the *cis*-platin molecule ($NH_3$–Pt–$NH_3$) by 5.869°; this can be interpreted in terms of the $CH_2$, which connects the two coordination sites and prevents opening of this angle. This bond angle is also larger than that of the palladium complex of the *p*-$NO_2$ derivative (Pd–$L^1$), 80.555° [2], and this may be attributed to the presence of an intramolecular H-bond between the secondary amino group and *o*-$COOCH_3$ in the *ortho*-position. The calculated Cl(23)–Pd–Cl(24) (92.969°) angle is slightly larger than the experimental one in *cis*-platin by 1.069° [20] and smaller than that reported for the palladium complex of the *p*-$NO_2$ derivative (94.889°) [2]. This may be attributed to the intermolecular H-bond between the Cl(24) and $H_2O$, O(51)–H(49)$\cdots$Cl(24), preventing opening of this angle.

A number of experimental and computational studies have focused on the classification of hydrogen bonds [21]. The conventional H-bond is defined as A–H$\cdots$B, where A and B are electronegative atoms such as nitrogen, oxygen, or halogen. This type of H-bond is observed in the studied optimized structure of *cis*-$[PdLCl_2]\cdot 2H_2O\cdot C_2H_5OH$, where the oxygen (O52) of water interacts directly with the imidazolic N17–H35 forming an intermolecular hydrogen bond (1.725 Å). The other water molecule interacts with the palladium complex through two hydrogen bonds, one with coordinated chloride (Cl24) with O(51)–H(49)$\cdots$Cl(24) distance 2.393 Å and the other with the acidic proton (H34) of the secondary amino group with O(51)–H(34)$\cdots$N(19) distance 2.402 Å, as shown in figure 1. It should be emphasized that H34 participates also in an intramolecular hydrogen bond between oxygen (−0.657e) of the carbonyl and $NH_{sec}$ (−0.675e) [6]. Generally, formation of an H-bond results in elongation of the X–H bond and a broadening of the X–H stretching potential, which causes red shifts of the X–H stretching frequencies. Thus, the imidazolic NH (N(17)H(35)) bond length increases by 0.02221 Å in the Pd–L complex, in comparison with that of the anhydrous complex, due to participation of the latter group in an intermolecular H-bond with a water molecule.

Another type of H-bonding is the blue-shifting hydrogen bond, usually C–H$\cdots$B, where B is either an electronegative atom carrying one or more electron lone pairs or a region of excess electron density ($\pi$ electrons of an aromatic system) [21]. As shown in figure 1, the ethanol in $[PdLCl_2]\cdot 2H_2O\cdot C_2H_5OH$ forms double intermolecular H-bonds with the uncoordinated ester. The first is between the alcoholic oxygen (O45) and hydrogen of the methyl ester (H31) with a hydrogen bond distance of 2.314 Å, and the second H-bond comes from the interaction of the methylene group (H47) with the oxygen of the carbonyl (O20) with a distance of 2.281 Å. Linear H-bonds and those that approach linearity are usually stronger than bonds where the X–H$\cdots$Y angle is far from 180° [22]. Thus, the strongest H-bond in the Pd–L complex is N(17)–H(35)$\cdots$O(52), since the angle of this interaction is 177.15°.

To account for the effect of the water molecule of hydration and ethanol on the optimized structures of the studied complexes in terms of intermolecular interactions, the optimized structures of $[PdLCl_2]$ and $[PtLCl_2]$ were also obtained. H-bond energies

were computed as the difference in energy between the H-bonded complex on one hand (e.g. $[PdLCl_2]\cdot 2H_2O\cdot C_2H_5OH$) and the sum of isolated compounds on the other hand ($[PdLCl_2]$, $2H_2O$, and $C_2H_5OH$). It was found that the presence of one ethanol molecule in $[PdLCl_2]\cdot 2H_2O\cdot C_2H_5OH$ increases the stability of the palladium complex by 155.028 a.u., and this stability is enhanced by 152.873 a.u. due to the participation of two water molecules of hydration in the molecular structure of the investigated complex. According to calculations, important variations in partial charges are observed when going from individual $[MLCl_2]$ molecules to their H-bonded complexes with ethanol and water molecules. The optimized Pd–$N_{py}$ and Pd–$NH_{sec}$ bond lengths in $[PdLCl_2]\cdot 2H_2O\cdot C_2H_5OH$ are shorter than the corresponding ones in $[PdLCl_2]$ by 0.013 and 0.014 Å, respectively, as a result of charge redistribution on the two nitrogen atoms, where the charges on N18 and N19 are decreased by 0.031e and on the palladium by 0.344 e. The optimized Cl(24)–Pd bond length is only influenced (decreases by 0.025 Å) by the presence of intermolecular hydrogen, O(51)–H(49)$\cdots$Cl(24), as previously mentioned.

### 3.2. *NBO analysis*

The NBO calculation [13] of *cis*-$[PtLCl_2]\cdot C_2H_5OH$ was performed using NBO 3.1 implemented in the *GAUSSIAN 03* package at the DFT/B3LYP/LANL2DZ level. The ideal Lewis structure is constructed from Lewis $\sigma$-type (donor) NBOs that are complemented by the non-Lewis $\sigma$-type (acceptor) NBOs. The filled NBOs of the natural Lewis structure are well adapted to describe covalent effects in molecules. The anti-bonding orbitals represent empty valence-shell capacity and spanning portions of the atomic valence space that are formally unsaturated by covalent electrons. Weak occupancies of the valence anti-bond signal the irreducible departure from an idealized localized Lewis picture, i.e., true "delocalization effects." Therefore, the NBO analysis provides an efficient method for studying intra- and intermolecular bonding and provides a convenient basis for investigating charge transfer or conjugative interaction in molecular systems.

Table 1 collects the natural charges on the atoms. It is clear that the largest negative charges are located on the two nitrogen atoms, N(18) (−0.520e) and N(19) (−0.676e). According to NBO results, the electron configuration of Pt is [core]$6s^{0.55}$ $5d^{8.76}6p^{0.37}6d^{0.01}$. Thus, 67.99 core electrons, 9.68 valence electrons (on 6s, 5d, and 6p atomic orbitals), and 0.01 Rydberg electrons (on 6d orbital) give the 77.689 electrons. The calculated natural charge on the platinum atom in $[PtLCl_2]\cdot C_2H_5OH$ is +0.311 (difference between 77.689e and the total number of electrons in the isolated Pt atom (78e)), reducing significantly from the formal charge +2 as a consequence of electron density donation from the pyridine-type nitrogen, secondary amino, and two chlorides. The two chlorides (Cl(22) and Cl(23)) coordinated to platinum have lower negative charge −0.398e and −0.423e, respectively, compared to those reported for the palladium complex of the *p*-$NO_2$ derivative [2]. This may be attributed to an intermolecular H-bond between the complex and ethanol. For $[PdLCl_2]\cdot 2H_2O\cdot C_2H_5OH$, the electron configuration of Pd is [core]$5s^{0.35}4d^{8.92}5p^{0.38}5d^{0.01}6p^{0.01}$, with 35.99 core electrons, 9.65 valence electrons (on 5s, 4d, and 5p atomic orbitals), and 0.02 Rydberg electrons (mainly on 5d and 6p orbitals), giving total 45.654 electrons.

Table 2. Occupancy of natural orbitals (NBOs) and hybrids calculated for *cis*-$[PtLCl_2]\cdot C_2H_5OH$.

| Donor[a] Lewis-type NBOs (A–B) | Occupancy | Hybrid[b] | AO (%)[c] | Acceptor[d] non-Lewis NBOs | NBOs |
|---|---|---|---|---|---|
| σ(C(7)–N(17)) | 1.982 | $sp^{2.24}$ (C(7)) | s(30.88)p(69.12) | σ*(C(7)–N(17)) | 0.03219 |
| σ(C(7)–N(17)) | | $sp^{1.84}$ (N(17)) | s(35.16)p(64.84) | | |
| σ(C(7)–N(18)) | 1.977 | $sp^{2.14}$ (C(7)) | s(31.89)p(68.11) | σ*(C(7)–N(18)) | 0.027 |
| σ(C(7)–N(18)) | | $sp^{1.76}$ (N(18)) | s(36.30)p(63.70) | | |
| σ(Pt–Cl(22)) | 1.972 | $sp^{0.27}d^{1.23}$ (Pt) | s(39.99)p(10.64)d(49.37) | σ*(Pt–Cl(22)) | 0.225 |
| σ(Pt–Cl(22)) | | $sp^{5.85}$ (Cl) | s(14.61)p(85.39) | | |
| σ(Pt–Cl(23)) | 1.971 | $sp^{0.34}d^{1.28}$ (Pt) | s(38.16)p(12.95)d(48.89) | σ*(Pt–Cl(23)) | 0.229 |
| σ(Pt–Cl(23)) | | $sp^{5.34}$ (Cl) | s(15.78)p(84.22) | | |
| σ(N(17)–H(34)) | 1.988 | $sp^{2.37}$ (N(17)) | s(29.68)p(70.32) | σ*(N(17)–H(34)) | 0.017 |
| σ(N(19)–H(33)) | 1.966 | $sp^{2.09}$ (N(19)) | s(32.35)p(67.65) | σ*(N(19)–H(33)) | 0.061 |
| π(C(15)–O(20)) | 1.979 | $sp^{99.99}$ (C(15)) | s(0.12)p(99.88) | π*(C(15)–O(20)) | 0.023 |
| π(C(15)–O(20)) | | $sp^{99.99}$ (O(20)) | s(0.12)p(99.88) | | |
| LP(1)–N(18) | 1.650 | $sp^{2.50}$ | s(28.56)p(71.44) | RY*(1) N18 | 0.007 |
| LP(1)–N(19) | 1.658 | $sp^{7.72}$ | s(11.46)p(88.54) | RY*(1) N19 | 0.006 |
| LP(1)–O(20) | 1.965 | $sp^{0.6}$ | s(62.63)p(37.37) | RY*(1)Pt | 0.0022 |
| LP(2)–O(20) | 1.860 | $sp^{48.05}$ | s(2.04)p(97.96) | RY*(2)Pt | 0.0017 |
| LP(1)–Pt | 1.988 | $sp^{0.04}d^{43.31}$ | s(2.25)p(0.09)d(97.66) | RY*(3)Pt | 0.0016 |
| LP(2)–Pt | 1.986 | $sp^{0.01}d^{26.69}$ | s(3.61)p(0.05)d(96.34) | RY*(4)Pt | 0.0015 |
| LP(3)–Pt | 1.978 | $sp^{0.10}d^{99.99}$ | s(0.63)p(0.06)d(99.31) | RY*(5)Pt | 0.0011 |

[a]LP(n)A is a valence lone pair orbital (n) on A atom.
[b]Hybrid on A atom in the A–B bond or otherwise, as indicated.
[c]Percentage contribution of atomic orbitals in NBO hybrid.
[d](*) denotes antibonding, and Ry corresponds to the Rydberg NBO orbital.



Table 2 lists the calculated occupancies of natural orbitals. Three classes of NBOs are included, the Lewis-type (s and p bonding or lone pair) orbitals, the valence non-Lewis (acceptors, formally unfilled) orbitals, and the Rydberg NBOs, which originate from orbitals outside the atomic valence shell. The calculated natural hybrids on atoms are also given in this table. The σ(Pt–Cl(22)) bond is formed from an $sp^{0.27}d^{1.23}$ hybrid on platinum (which is the mixture of 39.99% s, 10.64% p, and 49.37% d atomic orbitals) and $sp^{5.85}$ hybrid on chloride (85.39% p contribution). The NBO results show that the σ(Pt–Cl(22)) bond is strongly polarized towards chloride with about 72.98% of electron density concentrated on the chloride. The polarization of σ(Pt–Cl(22)) bond is affected by the intermolecular H-bond between chloride and water as compared with that found in the platinum complex of the *p*-$NO_2$ derivative [2]. This interaction leads to increasing the population of the p-orbital on platinum and decreasing that of chloride. Similarly, the σ(Pd–Cl(23)) bond is formed from an $sp^{0.34}d^{1.32}$ hybrid on palladium (which is the mixture of 37.60% s, 12.82% p, and 49.58% d atomic orbitals) and $sp^{7.51}$ hybrid on chloride (88.25% p contribution). Thus the σ(Pd–Cl(23)) bond is also strongly polarized toward chloride with about 75.01% of electron density concentrated on chloride.

Table 3 lists the selected values of the calculated second-order perturbation theory analysis of Fock Matrix in NBO basis between donor and acceptor orbitals in the $[PtLCl_2]\cdot C_2H_5OH$ complex. The strongest interactions are electron donations from a lone pair orbital on nitrogen, LP(1)N(18) (71.44% p, ED ≈ 1.650 e) and LP(1)N(19) (88.54% p, ED ≈ 1.658 e) to the anti-bonding acceptor σ*(Pt–Cl(23)) and σ*(Pt–Cl(22)) orbitals, respectively: LP(1)N(18) → σ*(Pt–Cl(23)) and LP(1)N(19) → σ*(Pt–Cl(22)). This mechanism can explain a relatively high occupancy of σ*(Pt–Cl(22)) and σ*(Pt–

Table 3. Second-order interaction energy ($E^2$, kcal mol$^{-1}$) between donor and acceptor orbitals in *cis*-[PtLCl$_2$]•C$_2$H$_5$OH (selected).

| Donor→Acceptor | $E^2$ | Donor→Acceptor | $E^2$ |
|---|---|---|---|
| LP(1)N(17) → $\sigma^*$(C(7)–N(18)) | 59.85 | LP(1)N(19) → $\sigma^*$(Pt–Cl(22)) | 34.22 |
| LP(2)O(21) → $\sigma^*$(C(15)–O(20)) | 54.41 | $\sigma$(Pt–Cl(22)) → $\sigma^*$(Pt–Cl(23)) | 4.28 |
| LP(1)N(18) → RY*(5)Pt | 42.32 | $\sigma$(Pt–Cl(23)) → $\sigma^*$(Pt–Cl(22)) | 3.58 |
| LP(1)N(18) → $\sigma^*$(Pt–Cl(23)) | 40.51 | LP(2)O(48) → $\sigma^*$(C(16)–H(29)) | 4.29 |
| LP(1)N(19) → RY*(6)Pt | 32.49 | | |



Cl(23)) anti-bonding orbitals. A gain of occupancy in anti-bonding acceptor orbital is directly correlated with a weakening of the bond associated with this orbital.

Alternatively, the lone pair interaction LP(2)O48 with anti-bonding $\sigma^*$(C(16)–H(29)) is evidence for charge transfer from ethanol to platinum. Similarly, charge transfer found in [PdLCl$_2$]·2H$_2$O·C$_2$H$_5$OH confirms the presence of intermolecular H-bonds as LP(1)O(20) → $\sigma^*$(C(41)–H(47)), LP(3)Cl(24) → $\sigma^*$(H(49)–O(51)), LP(2)O(51) → $\sigma^*$(N(19)–H(34)), and LP(2)O(52) → $\sigma^*$(N(17)–H(35)) with energies of 1.50, 7.49, 1.11, and 24.55 k cal mol$^{-1}$, respectively. This confirms that the strongest H-bond is found between water and imidazolic, as previously mentioned.

### 3.3. *Electronic structure and FMO*

The FMOs play an important role in electronic and optical properties [23]. The frontier orbital gap helps characterize the chemical reactivity and kinetic stability of the molecule. A molecule with a small frontier orbital gap is more polarizable, generally associated with a high chemical reactivity, low kinetic stability, and is termed a soft molecule. The frontier orbital energies ($E_{HOMO}$ and $E_{LUMO}$) are important parameters of molecular electronic structure. The lowest HOMO energy shows that molecule donating electron ability is the weakest. On the contrary, the highest HOMO energy implies that the molecule is a good electron donor. LUMO energy presents the ability of a molecule receiving electron. Figure 2 shows the distribution and energy levels of the HOMO and LUMO orbitals for the studied complexes. The values of the energy separation between the HOMO and LUMO are 3.582 and 3.477 eV for *cis*-[PdLCl$_2$]·2H$_2$O·C$_2$H$_5$OH and *cis*-[PtLCl$_2$]·C$_2$H$_5$OH, respectively.

The electronic spectrum of the benzimidazole L displayed four absorptions in DMF at 263, 275, 281, and 340 nm [6]. In complexes, the bands at 270, 280, and 345 nm are assigned to internal ligand transitions. Moreover, the first low-energy spin-allowed band at 21,505 cm$^{-1}$ ($\Delta_1 = 22{,}508$ cm$^{-1}$, $\log \varepsilon_{max} = 3.18$) in Pd–L complex is assigned to the transition $^1A_{1g} \rightarrow {}^1A_{2g}$ ($\nu_1$). The band at 23,041 cm$^{-1}$ ($\log \varepsilon_{max} = 2.95$) in the Pd–L complex and 24,038 cm$^{-1}$ ($\log \varepsilon_{max} = 3.34$) in the Pt–L complex is assigned to $^1A_{1g} \rightarrow {}^1B_{2g}$ ($\nu_2$). The $\nu_2/\nu_1$ value for the Pd(II) complex is 1.07, comparable with values reported earlier for square-planar complexes [24]. Thus, the electronic spectra of these complexes are indicative of square-planar geometry [25].

The lowest 10 singlet-to-singlet spin-allowed excitation states were taken into account for the calculation of electronic absorption spectra of the investigated complexes using the TD-DFT method. The calculated energy of excitation states and transition

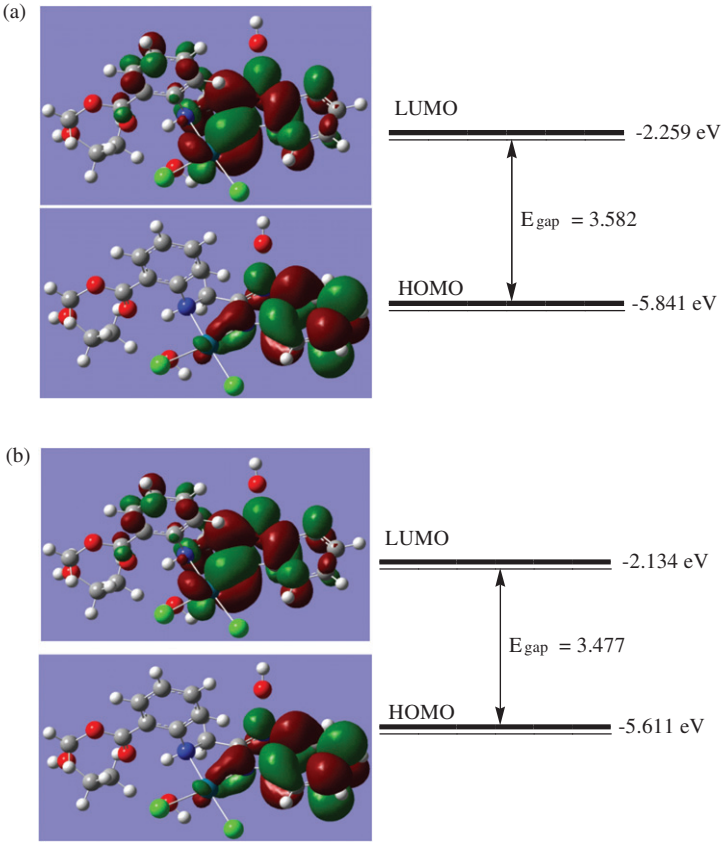


Figure 2. Molecular orbital surfaces and energy levels of (a) *cis*-$[PdLCl_2]\cdot 2H_2O\cdot C_2H_5OH$ and (b) *cis*-$[PtLCl_2]\cdot C_2H_5OH$.

oscillator strength (f) (only $f > 0.002$ is listed) of the studied compounds are tabulated in table 4. The absorption spectra were simulated using *GAUSSSUM* software [26] based on the obtained TD-DFT results. Each excited state was interpolated by a Gaussian convolution with full-width at half-maximum (FWHM) of 3000 $cm^{-1}$. As shown in table 4, the theoretical UV-Vis spectrum of the Pd–L complex in the gaseous state is characterized by four bands ($f > 0.002$) at 341, 366, 432, and 541 nm, while five bands at 362, 374, 382, 409, and 431 nm distinguish the spectrum of the Pt–L complex.

### 3.4. *Vibrational assignments*

The theoretical IR spectra of the benzimidazole L and its Pd(II) and Pt(II) complexes were obtained at the DFT/B3LYP level of theory combined with the LANL2DZ basis set. The experimental and theoretical wavenumbers are given in the "Supplementary material." In these tables, the relative intensities of the vibrational bands, expressed as percentage of the most intense band in the corresponding spectrum are also given. Although the relative intensities are not very well predicted for all IR bands, they still

Table 4. Computed excitation energies (eV), electronic transition configurations and oscillator strengths (f) of the studied complexes (transitions with $f > 0.002$ are listed).

| nm (eV) | $f$ | Composition |
|---|---|---|
| *cis*-[$PtLCl_2$] · $C_2H_5OH$ | | |
| 431 (2.877) | 0.0071 | H–2→L (16%), H–2→L + 2 (17%), H–1→L (24%), H–1→L + 2 (14%), H–3→L (3%), H–3→L + 2 (8%), H–2→L + 3 (2%), H–1→L + 1 (3%), H→L + 2 (4%) |
| 409 (3.028) | 0.0033 | H→L (35%), H→L + 2 (43%), H–1→L + 2 (4%), H→L + 1 (8%), H→L + 3 (4%) |
| 382 (3.242) | 0.0073 | H–2→L (32%), H–2→L + 2 (24%), H–1→L (13%), H–1→L + 2 (10%) |
| 374 (3.314) | 0.0112 | H–1→L + 1 (19%), H→L + 1 (65%), H–1→L + 2 (3%), H→L + 2 (9%) |
| 362 (3.417) | 0.0124 | H–3→L (64%), H–3→L + 2 (28%), H–3→L + 3 (4%) |
| *cis*-[$PdLCl_2$] · $C_2H_5OH \cdot 2H_2O$ | | |
| 541 (2.292) | 0.0026 | H–4→L (12%), H–1→L (53%), H→L (11%), H–18→L (2%), H–3→L (4%), H–1→L + 1 (7%) |
| 432 (2.872) | 0.0056 | H–4→L (12%), H–3→L (60%), H–1→L (18%) |
| 366 (3.384) | 0.0031 | H–2→L + 1 (10%), H→L (11%), H→L + 1 (74%) |
| 341 (3.638) | 0.0173 | H–4→L + 1 (60%), H–3→L + 1 (25%), H–4→L (9%), H–3→L (3%) |

provide useful help for the assignment of the normal modes in the experimental spectra. Calculated harmonic frequencies by DFT are usually higher than the corresponding experimental quantities due to the electron correlation approximate treatment, anharmonicity effects, basis set deficiencies, etc. [27]. To compensate these shortcomings, scale factors were introduced and an explanation of this approach was discussed [28]. Thus, a *uniform* scaling method with a scaling factor 0.970 is introduced. Experimentally, the sharp band at 3345 $cm^{-1}$ in the FT-IR spectrum of L is assigned to $\nu(NH_{sec})$ and this vibration mode is located at lower wavenumber than that of (1H-benzimidazol-2-ylmethyl)-(4-nitro-phenyl)-amine [2] due to an intramolecular H-bond between this group and O–$COOCH_3$, N(25)–H(28) ··· O(24) [6]. In complexes, this group falls under two effects, the withdrawal effect of the nitrogen, as a result of complex formation, and the intramolecular hydrogen bonding, N(25)–H(28) ··· O(24). These two effects compensate each other, leading to higher wavenumbers than that of the free ligand, 3352 $cm^{-1}$ for Pd–L and 3375 $cm^{-1}$ for Pt–L. Theoretically, participation of the $NH_{sec}$ group in the coordination sphere of the studied complexes is confirmed by observing the scaled $\nu(NH_{sec})$ vibration mode at lower wavenumbers, 3209 and 3144 $cm^{-1}$ for Pd–L and Pt–L complexes, respectively, than that of the free ligand (3367 $cm^{-1}$).

The band at 1674 $cm^{-1}$ in the free ligand is assigned to $\nu$(C=O) [6]. In complexes, the carbonyl group is not involved in coordination since its stretching mode is located at higher wavenumbers than that of the free ligand [29], as shown in the "Supplementary material." Experimentally, it is difficult to assign the $\nu(NH_{Bz})$ in the free ligand [2, 6] owing to the presence of the intermolecular hydrogen bond, N(12)–H(36) ··· N(11). This group is still masked in the spectra of metal complexes due to the hydrogen bond effect generated by water and ethanol. The calculated scaled value at 3571 $cm^{-1}$ in the benzimidazole L and its Pt–L complex is assigned to $\nu(NH_{Bz})$, confirming that the $NH_{Bz}$ remains intact in the complexes. However, this vibrational mode is found at lower wavenumber (3194 $cm^{-1}$) in the Pd–L complex due to involvement in intermolecular hydrogen bonding with the water molecule (Supplementary material).

The far-IR spectrum of the Pd–L complex shows two medium bands at 368 and 362 $cm^{-1}$ due to $\nu$(Pd–Cl) in a *cis*-square planar structure [30]. Similarly, the platinum

complex shows these modes at 367 and 355 $cm^{-1}$. Theoretically, the scaled $\nu_{ss}$(Pd–Cl) and $\nu_{ass}$(Pd–Cl) modes are observed at 324 and 313 $cm^{-1}$, while the scissoring bending mode Cl–Pd–Cl is found at 132 $cm^{-1}$. For the Pt–L complex, the latter modes are established at 318, 311, and 140 $cm^{-1}$, respectively. In addition, the theoretically scaled vibrations at 330 and 235 $cm^{-1}$ in the Pd–L complex are assigned to Pd–$N_{py}$ and Pd–$NH_{sec}$, while bands at 271 and 216 $cm^{-1}$ are allocated for Pt–$N_{py}$ and Pt–$NH_{sec}$ in the Pt–L complex.

Calculated bands at 3758, 3599, and 1568 $cm^{-1}$ in the Pd–L complex are assigned to asymmetric, symmetric stretching, and scissoring modes of the water molecule that is attracted to the imidazolic NH. These vibration modes are found at 3662, 3432, and 1593 $cm^{-1}$ for the other water molecule. The theoretically scaled value at 3570 $cm^{-1}$ is assigned to $\nu$(OH) of ethanol in the Pd–L and Pt–L complexes. The RMS error of the frequencies between the unscaled and experimentally observed in L was 64 $cm^{-1}$. After scaling, the RMS values are 20 $cm^{-1}$ for L, 33 $cm^{-1}$ for Pd–L, and 14 $cm^{-1}$ for Pt–L complexes. Therefore, FT-IR study reveals that L is coordinated to the Pd(II) and Pt(II) only *via* the pyridine-type nitrogen ($N_{py}$) of the benzimidazole ring and secondary amino group ($NH_{sec}$) in a square-planar geometry.

### 3.5. *$^1$H-NMR studies*

The $NH_{Bz}$ is at 12.35 ppm [6] in L and moves downfield in its complexes, 13.36 ppm for Pd–L and 13.27 ppm for Pt–L complex. This shift is related to the electron density change in the benzimidazole ring, which supports coordination *via* the pyridine nitrogen. The triplet at 8.30 ppm is due to $NH_{sec}$, whereas the doublet at 4.68 ppm is assigned to $CH_2$ in the free ligand [6]. In complexes, both signals move downfield owing to participation of $NH_{sec}$ in chelation. The methylene-protons are diastereotopic, resonating as a pair of quartets between 5.02 and 5.65 ppm. The benzimidazole (L) exhibits a singlet at 3.80 ppm due to protons of the methyl and this signal is still observed in the complexes at nearly the same position, 3.86 ppm for Pd–L and 3.88 for Pt–L. This confirms that the carbonyl remains in the complexes. Two additional signals at 4.32 and 1.36 ppm in the complexes are assigned to $CH_2$ and $CH_3$ of ethanol [31].

### 3.6. *Mass spectrometry*

The mass spectrum of Pt–L complex gives $M^+$ at *m*/*z* 546 due to $[PtLCl_2]^+$ followed by the exclusion of $CH_3$ and one Cl to provide a peak at *m*/*z* 497, as demonstrated in the "Supplementary material." The latter fragment at *m*/*z* 497 eliminates $CO_2$ to give a peak at *m*/*z* 450. For the Pd–L complex, the fragmentation pattern resembles the free ligand itself with two additional fragments at *m*/*z* 310 and 295 due to the formation of [Pd(benzimidazole$CH_2$)$Cl_2$] and [Pd(benzimidazole)$Cl_2$] fragments, respectively.

### 3.7. *Thermal analyses and kinetics studies*

The TG/DTA curves of Pd–L complex show two endothermic degradation steps at 283°C and 429°C, as shown in the "Supplementary material." The first stage is accompanied by a mass loss amounting to 32.94% (Calcd 32.69%). This value is from

the exclusion of $C_2H_5OH$, $2H_2O$, $CO_2$, $CH_3$, and Cl. Desorption of ethanol and water molecules at relatively high-temperature indicates participation of these molecules in hydrogen bonding [32], as discussed theoretically. The second pronounced step corresponds to the removal of the rest of organic part (L–$CH_3$–$CO_2$) and another chloride with a mass loss amounting to 47.23% (Calcd 47.69%), leaving Pd as a final residue at 1200°C. The simultaneous TG/DTA curves of the Pt–L complex show two endothermic decomposition steps at 289°C and 445°C. The first decomposition step is attributed to the loss of one ethanol, one chloride, and the benzimidazole. The second thermal step is due to the removal of another chloride and aniline moiety, leaving platinum metal as a residue with an overall weight loss amounting to 66.50% (Calcd 67.10%).



### 3.8. *X-ray powder diffraction*

Many trials have been done to isolate the single crystal of the investigated complexes, but all of them failed owing to the amorphous nature of these compounds, as confirmed by their XRD data. The X-ray powder diffraction patterns of the Pd–L and Pt–L complexes were recorded over $2\theta = 5–60^\circ$ to evaluate lattice dynamics of these compounds. The comparison between the obtained XRD patterns of L and its complexes (Supplementary material) show that each complex represents a definite compound with a distinct structure; identification of the complexes was done by the known method [33]. The studied complexes are amorphous.

### 3.9. *Biological activity*

**3.9.1. Antimicrobial activity.** The antimicrobial activities were carried out using the culture of *B. subtilis*, *S. aureus*, and *S. faecalis* as Gram-positive bacteria and *E. coli*, *P. aeruginosa*, and *N. gonorrhea* as Gram-negative bacteria. The data show that the complexes inhibit the metabolic growth of the investigated bacteria to different extents (figure 3). In earlier results [2], the activity of the ligands was slightly affected by the nature of the substituent in the *para* position of the aniline ring, and this was justified in terms of the lipophilicity of the ligands and their membrane permeability, a key factor in determining their entry inside the cells. Introduction of the *o*-$COOCH_3$ group (benzimidazole L) did not lead to a notable change in the biological activity compared with the *para*-2-arylaminomethyl-1H-benzimidazole derivative [2], i.e., the substituents have no significant role in the inhibition of the metabolic growth of the investigated organisms, and thus the activity of these compounds arises from the benzimidazole.

The L [6] is more toxic than the platinum complex, while the Pd–L complex is inactive. These results are in agreement with previously reported palladium complexes [2], confirming that the nature and position of the substituent on the aniline and the palladium itself have no marked affect on activities of the palladium complexes. The effectiveness of the benzimidazole L and its platinum complex against different organisms depends on the impermeability of the cells of the microbes or on differences in the ribosome of microbial cells. A possible explanation for the poor activity of these complexes in comparison with L may be their inability to chelate metals essential for the metabolism of microorganisms and/or to form hydrogen bonds with the active centers

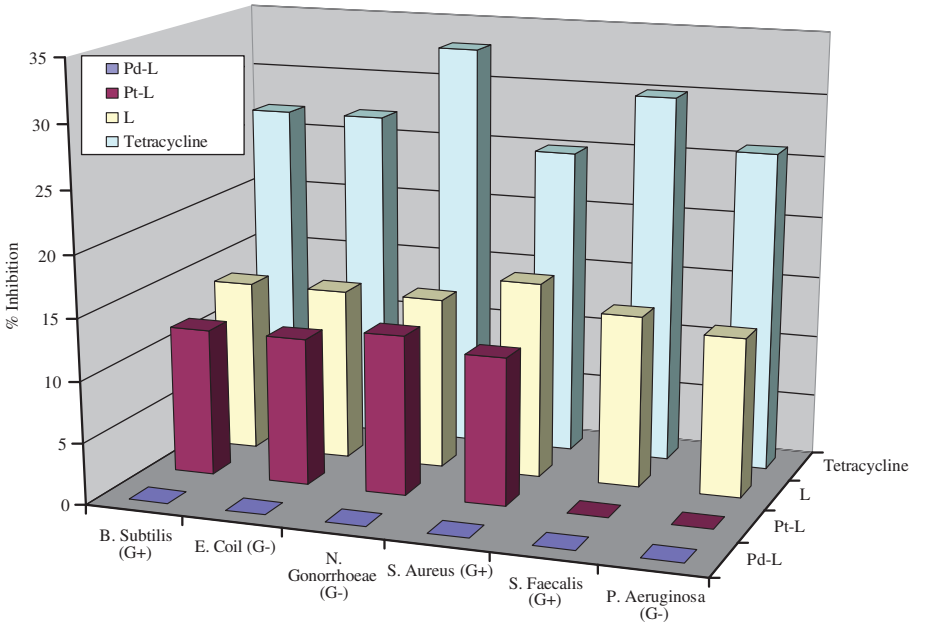


Figure 3. Antibacterial activities of ligand L and its complexes against *B. subtilis* (G1), *S. aureus* (G2), and *S. faecalis* (G3) as Gram-positive, (G4) *P. aeruginosa* (G4), *E. coli* (G5), and *N. Gonorrhea* (G6) as Gram-negative bacteria.

of cell structures, resulting in an interference with the normal cell cycle. It is also due to their low lipophilicity, where the penetration of the complex through the lipid membrane is decreased, and hence they cannot block or inhibit growth of the microorganism.

**3.9.2. Cytotoxicity.** To evaluate the potential usefulness of Pd–L and Pt–L complexes synthesized as antitumor agents, three cell lines of different origin, *breast cancer* (MCF7), *colon carcinoma* (HCT), and *human heptacellular carcinoma* ($HepG_2$), were treated. This experiment was performed at 100 µmol $L^{-1}$ and compared with that of *cis*-platin. The $IC_{50}$ (the concentration that inhibited 50% of the cellular proliferation) of these compounds and *cis*-platin were determined. According to Shier [34], compounds exhibiting $IC_{50}$ activity of 10–25 µg $mL^{-1}$ are weak anticancer drugs, while those of $IC_{50}$ activity between 5.00 and 10.00 µg $mL^{-1}$ are moderate, and compounds of activity below 5.00 µg $mL^{-1}$ are considered strong agents.

The complexes showed higher activity than *cis*-platin on screening against $HepG_2$ cells at 100 µmol $L^{-1}$. The Pd–L complex exhibits moderate antitumor activity with $IC_{50} = 15.8$ µmol $L^{-1}$ (equivalent to 8.37 µg $mL^{-1}$) compared to that of *cis*-platin ($IC_{50} = 11.9$ µmol $L^{-1}$, equivalent to 3.57 µg $mL^{-1}$). In addition, the Pd–L complex is more toxic than the Pt–L complex. The higher toxicity of Pd–L complex happens because the ligand-exchange behavior of platinum compound is quite slow and results in ligand-exchange reactions of minutes to days, rather than microseconds to seconds for many other coordination compounds. In addition, Pt(II) has a strong

thermodynamic preference for binding to S-donors and for this reason, one would predict that platinum compounds would never reach DNA, with many cellular platinophiles (S-donor ligands, such as glutathione and methionine) as competing ligands in the cytosol [35]. For MCF7 and HCT cells, the studied complexes are less toxic than *cis*-platin at 100 μmol $L^{-1}$. The results obtained can be useful in understanding the factors that influence the activity of the complexes and in supporting the general assumption that the relationship between the structure and activity is extremely complex.



## 4. Conclusion

Synthesis and characterization of 2-[(1H-benzimidazol-2-ylmethyl)-amino]-benzoic acid methyl ester and its new Pd(II) and Pt(II) complexes were achieved. The presence of one ethanol increases the stability of theses complexes. Important variations in partial charges were observed when going from individual molecules to their H-bonded complexes. Charge transfer as LP(1)O(20) $\rightarrow \sigma^*$(C(41)–H(47)) and LP(3)Cl(24) $\rightarrow$ $\sigma^*$(H(49)–O(51)) confirms the presence of an intermolecular H-bond. TD-DFT calculations help to assign the electronic transitions. Based on the elemental analysis, spectral, thermal, and molar conductance measurements, a square-planar geometry is suggested for the complexes with general formula, $[MLCl_2] \cdot zH_2O \cdot C_2H_5OH$ (M = Pd, z = 2; M = Pt, z = 0). The studied compounds inhibit metabolic growth of the investigated bacteria to different extents. In addition, the complexes are toxic against three cell lines of different origin and represent an interesting class of new compounds from the viewpoint of their physicochemical and structural properties. The $IC_{50}$ (μg $mL^{-1}$) values were twice those of the corresponding *cis*-platin.

## References

[1] Y. Parajó, J.L. Arolas, V. Moreno, Á. Sánchez-González, J. Sordo, R. de Llorens, F.X. Avilés, J. Lorenzo. *Inorg. Chim. Acta*, **362**, 946 (2009).
[2] N.T. Abdel-Ghani, A.M. Mansour. *J. Mol. Struct.*, **991**, 108 (2011); *Inorg. Chim. Acta*, **373**, 249 (2011).
[3] (a) V. Rajendiran, M. Murali, E. Suresh, S. Sinha, K. Somasundaram, M. Palaniandavar. *Dalton Trans.*, 148 (2008); (b) J. Mann, A. Baron, Y. Opoku-Boahen, E. Johansson, G. Parkinson, L.R. Kelland, S. Neidle. *J. Med. Chem.*, **44**, 138 (2001).
[4] E. Bouwmann, W.L. Driessen, J. Reedijk. *Coord. Chem. Rev.*, **104**, 143 (1990).
[5] K. Akdi, R.A. Vilaplana, S. Kamah, J.A.R. Navarro, J.M. Salas, F. González-Vílcheza. *J. Inorg. Biochem.*, **90**, 51 (2002).
[6] N.T. Abdel-Ghani, A.M. Mansour. *Spectrochim. Acta, Part A*, **81**, 754 (2011).
[7] A. Skoog, D.M. West. *Fundamentals of Analytical Chemistry*, Thomson, Brooks, Cole, New York (2004).
[8] A.D. Becke. *J. Chem. Phys.*, **98**, 5648 (1993).
[9] P.J. Hay, W.R. Wadt. *J. Chem. Phys.*, **82**, 270 (1985).
[10] M.J. Frisch, G.W. Trucks, H.B. Schlegel, G.E. Scuseria, M.A. Robb, J.R. Cheeseman, V.G. Zakrzewski, J.A. Montgomery, R.E. Stratmann, J.C. Burant, S. Dapprich, J.M. Millam, A.D. Daniels, K.N. Kudin, M.C. Strain, O. Farkas, J. Tomasi, V. Barone, M. Cossi, R. Cammi, B. Mennucci, C. Pomelli, C. Adamo, S. Clifford, J. Ochterski, G.A. Petersson, P.Y. Ayala, Q. Cui, K. Morokuma, D.K. Malick, A.D. Rabuck, K. Raghavachari, J.B. Foresman, J. Cioslowski, J.V. Ortiz, A.G. Baboul, B.B. Stefanov, G. Liu, A. Liashenko, P. Piskorz, I. Komaromi, R. Gomperts, R.L. Martin, D.J. Fox, T. Keith, M.A. Al-Laham, C.Y. Peng, A. Nanayakkara, C. Gonzalez, M. Challacombe, P.M.W. Gill,

B.G. Johnson, W. Chen, M.W. Wong, J.L. Andres, M. Head-Gordon, E.S. Replogle, J.A. Pople. *GAUSSIAN 03 (Revision A.9)*, Gaussian, Inc., Pittsburgh, PA (2003).
[11] A. Frisch, A.B. Nielson, A.J. Holder. *GAUSSVIEW User Manual*, Gaussian, Inc., Pittsburgh, PA (2000).
[12] M.E. Casida, J.M. Seminario (Eds). *Recent Developments and Applications of Modern Density Functional Theory, Theoretical and Computational Chemistry*, Vol. 4, p. 391, Elsevier, Amsterdam (1996).
[13] F. Weinhold, J.E. Carpenter. *The Structure of Small Molecules and Ions*, p. 227, Plenum, New York (1988).
[14] (a) D. Greenwood. *Antimicrobial Chemotherapy, Part II. Laboratory Aspects of Antimicrobial Therapy*, p. 71, Bailliere, Tindall, London (1983); (b) V. Lorian. *Antibiotics in Laboratory Medicine*, Williams & Wilkins, Baltimore (1996).
[15] National Committee for Clinical Laboratory Standards (NCCLS). *NCCLS Approval Standard Document M2-A7*, Vilanova, PA (2000).
[16] (a) P. Skehan, R. Smreng, D. Scudiero, A. Monks, J. McMahon, D. Vistica, J.T. Warren, H. Bokesch, S. Kenney, M.R. Boyd. *J. Nat. Cancer Inst.*, **82**, 107 (1990); (b) A. Monks, D. Scudiero, P. Skehan, R. Shoemaker, K. Paull, D. Vistica, C. Hose, J. Langley, P. Cronise, A. Vaigro-Wolff, M. Gray-Goodrich. *J. Nat. Cancer Inst.*, **83**, 757 (1991).
[17] C.M. Lozano, O. Cox, M.M. Muir, J.D. Morales, J.L. Rodríguez-Cabáin, P.E. Vivas-Mejfa, F.A. Gonzalez. *Inorg. Chim. Acta*, **271**, 137 (1998).
[18] D.N. Neogi, P. Das, A.N. Biswas, P. Bandyopadhyay. *Polyhedron*, **25**, 2149 (2006).
[19] (a) R.W. Hay, T. Clifford, P. Lightfoot. *Polyhedron*, **17**, 3575 (1998); (b) X. Jing-Yuan, G. Wen, L. Ling, Y. Shi-Ping, C. Peng, L. Dai-Zheng, J. Zong-Hui. *J. Mol. Struct.*, **644**, 23 (2003).
[20] R. Wysokiński, D. Michalska. *J. Comput. Chem.*, **22**, 901 (2001).
[21] P. Malla, D. Marion, E.V. Ivanova, H.M. Muchall. *J. Mol. Struct.*, **979**, 101 (2010).
[22] V. Chiş, A. Pîrnău, M. Vasilescu, R.A. Varga, O. Oniga. *J. Mol. Struct., (Theochem)*, **851**, 63 (2008).
[23] I. Fleming. *Frontier Orbitals and Organic Chemical Reactions*, Wiley, London (1976).
[24] (a) D.H. Basch, H.B. Gray. *Inorg. Chem.*, **6**, 365 (1967); (b) H.B. Gray, C.J. Ballhausen. *J. Am. Chem. Soc.*, **85**, 260 (1963).
[25] (a) A.B.P. Lever. *Inorganic Electronic Spectroscopy*, 2nd Edn, Elsevier, Amsterdam (1982); (b) D.X. West, M.S. Lockwood, A. Liberta, X. Chen, R.D. Willet. *Transition Met. Chem.*, **18**, 221 (1993).
[26] N.M. O'Boyle, A.L. Tenderholt, K.M. Langner. *J. Comp. Chem.*, **29**, 839 (2008).
[27] (a) G. Rauhut, P. Pulay. *J. Phys. Chem.*, **99**, 3093 (1995); (b) J.A. Pople, H.B. Schlegel, R. Krishnan, J.S. Defrees, J.S. Binkley, M.J. Frisch, R.A. Whiteside. *Int. J. Quantum Chem.: Quantum Chem. Symp.*, **15**, 269 (1981).
[28] (a) M.W. Ellzy, J.O. Jensen, H.F. Hameka, J.G. Kay, D. Zeroka. *Spectrochim. Acta*, **57A**, 2417 (2001); (b) J.O. Jensen, A. Banerjee, C.N. Merrow, D. Zeroka, J.M. Lochner. *J. Mol. Struct.: Theochem.*, **531**, 323 (2000); (c) J.O. Jensen, D. Zeroka. *J. Mol. Struct.: Theochem.*, **487**, 267 (1999).
[29] G. López, G. Sánchez, G. Garcia, M.J. Vidal. *Transition Met. Chem.*, **16**, 469 (1991).
[30] (a) J.R. Ferraro. *Low Frequency Vibrations of Inorganic and Coordination Compounds*, Plenum Press, NY (1971); (b) R.J.H. Clark, C.S. Williams. *Inorg. Chem.*, **4**, 350 (1965).
[31] R.M. Silverstein, F.X. Webster, D.J. Kiemle. *Spectroscopic Identification of Organic Compounds*, 7th Edn, John Wiley & Sons, New York (2005).
[32] S.A. Sadeek, M.S. Refat, H.A. Hashem. *J. Coord. Chem.*, **59**, 759 (2006).
[33] B.D. Cullity. *Elements of X-ray Diffraction*, 2nd Edn, Addison-Wesley Inc., Reading, MA (1993).
[34] W.T. Shier. *Mammalian Cell Culture on $5 a Day: A Lab Manual of Low Cost Methods*, p. 64, University of the Philippines, Los Banos (1991).
[35] M. Pérez-Cabré, G. Cervantes, V. Moreno, M.J. Prieto, J.M. Pérez, M. Font-Bardia, X. Solans. *J. Lnorg. Biochem.*, **98**, 510 (2004).